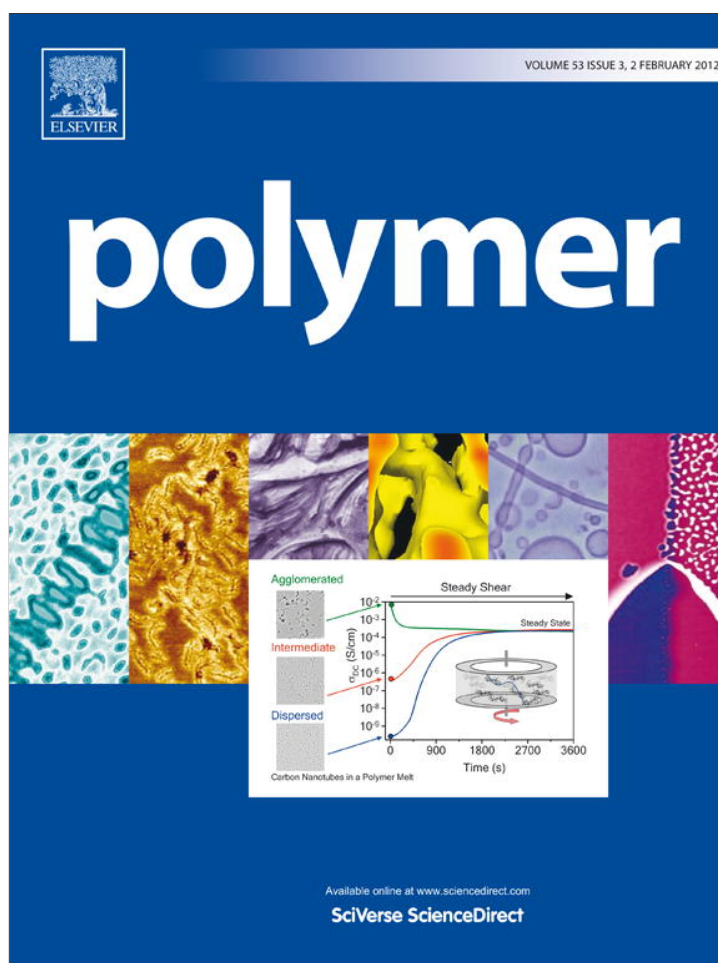


Provided for non-commercial research and education use.  
Not for reproduction, distribution or commercial use.



This article appeared in a journal published by Elsevier. The attached copy is furnished to the author for internal non-commercial research and education use, including for instruction at the authors institution and sharing with colleagues.

Other uses, including reproduction and distribution, or selling or licensing copies, or posting to personal, institutional or third party websites are prohibited.

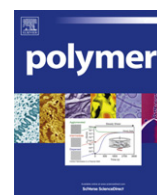
In most cases authors are permitted to post their version of the article (e.g. in Word or Tex form) to their personal website or institutional repository. Authors requiring further information regarding Elsevier's archiving and manuscript policies are encouraged to visit:

<http://www.elsevier.com/copyright>



Contents lists available at SciVerse ScienceDirect

Polymer

journal homepage: [www.elsevier.com/locate/polymer](http://www.elsevier.com/locate/polymer)

## Multiscale characterization of filler dispersion and origins of mechanical reinforcement in model nanocomposites

Nicolas Jouault<sup>a,b,\*</sup>, Florent Dalmas<sup>c</sup>, François Boué<sup>a</sup>, Jacques Jestin<sup>a,\*\*</sup>

<sup>a</sup>Laboratoire Léon Brillouin (LLB, CEA/CNRS), CEA Saclay, 91191 Gif-sur-Yvette Cedex, France

<sup>b</sup>Laboratoire d'Ingénierie des Matériaux de Bretagne (LIMATB), Université de Bretagne Sud, Centre de Recherche, Rue Saint Maudé, BP 92116, 56321 Lorient cedex, France

<sup>c</sup>Institut de Chimie et des Matériaux Paris-Est (ICMPE), UMR 7182, CNRS/Université Paris-Est Créteil, 2-8 rue Henri Dunant 94320 Thiais, France

### ARTICLE INFO

#### Article history:

Received 21 July 2011

Received in revised form

3 October 2011

Accepted 2 December 2011

Available online 8 December 2011

#### Keywords:

Nanocomposites

Filler dispersion

Small angle scattering (X-rays and neutrons)

### ABSTRACT

We report on the influence of parameters controlling filler dispersion and mechanical reinforcement in model nanocomposites. We elaborate a series of nanocomposites and present a structural characterization of silica dispersion in polymer matrix for several particle sizes and polymer matrices, at all relevant scales, by coupling Small Angle X-ray Scattering and Transmission Electronic Microscopy. The mechanical properties are investigated in the linear regime by coupling Dynamical Mechanical Analysis and plate/plate rheology. The results show that: (i) for all filler sizes and matrices, a structural transition is observed from non-connected fractal aggregates at low silica concentration to connected network at high particle content. (ii) In the dilute regime, the reinforcement implies a polymer chain contribution with different possible origins: increase of entanglements density for PS and increase of friction coefficient for PMMA. (iii) In the concentrated regime, for a given polymer, the reinforcement amplitude can be tuned by the rigidity of the filler network, which directly depends on the particle–particle interaction.

© 2011 Elsevier Ltd. All rights reserved.

### 1. Introduction

The design of polymer nanocomposites (PNCs) results in many opportunities for implementations in material science since the inclusion of nanoparticles (NPs) in polymeric matrix confers to them a number of properties for various practical applications and for fundamental insights [1]. The increase of surface to volume ratio thanks to the size of small NPs leads to the improvement of properties in nanocomposites compared to pure polymers or macro-composites and the combination of different NPs (carbon-based widely used, oxides, silica, metals...) with different polymers makes possible to design materials and finely modulate their final properties (rheological, optical, dielectric...) [2].

In this context, the mechanical reinforcement of amorphous polymers by the addition of NPs (fillers) is very efficient but its mechanisms need more comprehensive explanations: it still appears as a complex phenomenon that depends on two main questions: how do arrange the fillers in the polymer (the filler

dispersion) and how the fillers and the polymer interact [3]. The mechanisms involved in reinforcement are system dependent, i.e. influenced by the nature of the fillers (size, shape, aspect ratio) and the nature of the polymer (interaction potential with fillers). On the one hand, many filler morphologies at various length scales are encountered in polymeric matrix due to the complex interactions between fillers and polymer [4]: well dispersed particles, fractal aggregates, filler network or large agglomerates. These various structures enable variations in reinforcement [5], different from the classical hydrodynamic one: from high reinforcement (high modulus and large deformability) due to direct interactions between fillers, to “poor” reinforcement (increase of modulus but also of sample fragility) with too large aggregates. The reinforcement appears particularly more efficient when particles arrange in complex structured aggregates rather than they are perfectly dispersed [6]. But the precise relationship between such NPs dispersion and mechanical behavior involve many criterions and remains to be understood. On the other hand, changes in mechanical properties can be correlated to the nature of polymer/filler interaction through the modification of the local structure of the polymer. Properties of the polymer at the interface can greatly differ from the bulk polymer: the increase of the number of contacts between fillers and polymer (chain anchoring) or of the chain entanglements may lead to an increase of local segmental packing. Such interaction seems to modify the polymer dynamics

\* Corresponding author. Present address: Laboratoire Matière et Systèmes Complexes (MSC), UMR 7057, Université Paris 7-Diderot, 75205 Paris cedex 13, France.

\*\* Corresponding author.

E-mail addresses: [nicolas.jouault@univ-paris-diderot.fr](mailto:nicolas.jouault@univ-paris-diderot.fr) (N. Jouault), [jacques.jestin@cea.fr](mailto:jacques.jestin@cea.fr) (J. Jestin).

over large length scales: it undergoes changes of chain dynamic [7] which can be interpreted as leading to a gradient of local glass transition  $T_g$  from filler surface to the bulk [8]. The existence of glassy regions inside the melt matrix has also been proposed to explain the enhanced reinforcement in nanocomposites [9], with even, in specific cases, the formation of glassy paths, which percolate and create a continuous network [10].

Nevertheless, these two contributions are intimately associated and involve interdependent parameters difficult to de-correlate in experimental approaches. Nowadays some systems have been synthesized in which we can study separately these two contributions with one remaining question: what factors control the filler dispersion and thus the mechanical properties? One factor could be the relative polymer/NPs sizes: Mackay et al. [11] suggested earlier that the dispersion is controlled by the size ratio between polymer and filler  $R/R_g$ . The dispersion of nanoparticles is observed to increase when the radius of gyration of the polymer is greater than the size of the nanoparticles.

One strategy to modulate the dispersion is to graft polymer chains onto particles surface [12,13]. The surface modification of inorganic particles by organic molecules or by grafted chains should decrease the surface tension of a particle in a polymer melt, and therefore influence the filler spatial distribution [14] and thus the mechanical reinforcement. NPs grafted with polymer chains arrange in different self-assemblies depending on the molecular weight ratios between grafted and matrix polymers and on the grafting density. The tuning of these parameters leads to the creation of a “phase diagram” for the polymer/NPs mixtures [12,15]: NPs can form chains, branched objects or more complex anisotropic structures. Along the same lines it was then proposed that a significant reinforcement is obtained through the percolation of particles via grafted chains [16]. But, even with the best combinations of grafting and matrix for good dispersion, others external parameters (drying method, solvent, concentration, processing temperature) remain also important in the final dispersion and mechanical response.

Thus, another way to control the filler dispersion is to act on nanocomposites preparation. A number of processing techniques (melt mixing, solvent casting, extrusion and compression molding [17]) have been used to prepare PNCs leading to various dispersions. For solvent casting, Sen et al. [18] observed the influence of quality of the solvent used and evaporation rate on silica/polystyrene (PS) nanocomposites. At variance with “poor dispersion” (large agglomerates) where a  $T_g$ 's decrease is measured [19], a better dispersion is achieved when solvent is quickly evaporated, and no change in  $T_g$  is observed. These effects on  $T_g$  have been interpreted as due to the fact that the polymer/filler interface is affected by the process.

Recently we studied the silica/PS nanocomposites prepared by solvent casting and investigated the relation between filler morphology and the mechanical properties above  $T_g$  [20]. We have reported that (i) at high particle concentration there is a direct correlation between the local connected filler network and the fast increase of the reinforcement factor (ii) at low particle concentration, an important increase of the relaxation times (analogous to a solid-like behavior) is observed and cannot be directly attributed to interaction between fillers due to the longer inter-fillers distances, suggesting some polymer/filler interaction.

Here we extend this previous work and propose, keeping unchanged the casting process, to see whether the filler dispersion and the associated mechanical reinforcement are affected by the particles size and the matrix nature. First, following Mackay et al. [11], we can scan the phase diagram of silica dispersion by changing the particle size (in our case by increasing the radius by a factor 2). Second, changing the polymer matrix enables to modify the interaction between polymer and NPs and tune the strength of the

interfacial interaction and thus the filler morphology. In this context, polystyrene (PS) and polymethylmethacrylate (PMMA) have been chosen as two matrices because of their different reactivity with silica NPs. PMMA is known to adsorb strongly on NPs through hydrogen bonding between carboxyl groups and silanol groups. PS is known to weakly adsorb through dipole–dipole interaction of the benzene ring with the silica surface. Tannenbaum et al. [21,22] proposed that the number of possible anchoring points per chain  $\delta$  at the silica surface varies as  $\delta \propto M_w^{5/3}$  for PMMA and as  $\delta \propto M_w$  for PS with saturation for  $\delta$  at high  $M_w$ . Then, they provided a relation between its interfacial behavior and the mechanical properties and observed a power law dependence of the relative elastic modulus  $G_{rel}$  as  $G_{rel} \propto \delta^{1/3}$ .

Hence, the present study has two aims: the first one is to establish the filler structure adopted by the different silica beads in two amorphous polymer matrices through Small Angle X-rays Scattering (SAXS) and Transmission Electronic Microscopy (TEM) images. The second aim is to highlight the relation between morphology and reinforcement in order to identify the key parameters controlling both filler dispersion and mechanical properties at low deformation in the linear regime. We want to identify the main contribution dominating the reinforcement as a function of silica volume fraction, silica size and type of polymer. In the same time, in order to quantify the influence of processing conditions, we also follow the silica aggregation during nanocomposites processing by Small Angle Neutron Scattering (SANS).

## 2. Experimental

### 2.1. Nanocomposites processing

Nanocomposites were prepared by mixing nanosilica suspension, initially dispersed in an organic solvent, the DiMethylAcetamide (DMAc), with a polymer solution (10%v/v). The mixture is stirred for 2 h and then poured into Teflon moulds and let cast in an oven at constant temperature (130 °C) during 8 days to insure complete solvent evaporation. At the end we obtained dry films of dimension of 5 cm × 5 cm × 0.1 cm. Six model nanocomposites have been prepared with two polymer matrices (polystyrene (PS) with  $M_w/M_n = 2$  and polymethylmethacrylate (PMMA) with  $M_w/M_n = 2$ ) and three different silica beads. Both polymers have been purchased by Sigma Aldrich with an average molecular weight  $M_w$  of 280,000 g/mol and 350,000 g/mol for PS and PMMA respectively. Three different silica beads have been used to study the influence of size and polydispersity on dispersion and reinforcement. One silica solution already dispersed in DMAc (Nissan-St) was purchased by Nissan Chemical and two other silica suspensions were purchased by Sigma Aldrich, as initially dispersed in water (Ludox TM-40 and Ludox LS) and then subsequently transferred in DMAc by mixing and evaporation. Ludox silica dispersion remains stable during this transfer process: we compared SAXS curves in water before and after transfer in DMAc (SAXS measurements in water are not shown here) and the curves well superimpose: the particles are well dispersed in the organic solvent; we do not observe any aggregation due to the change of the solvent.

### 2.2. SANS and SAXS measurements

Small Angle Neutron Scattering (SANS) measurements were carried out on PAXY beamline at the Laboratoire Léon Brillouin (LLB). Three configurations sample to detector distance/wavelength were used:  $\lambda = 12 \text{ \AA}$  at 6.7 m,  $\lambda = 6 \text{ \AA}$  at 6.7 m and  $\lambda = 6 \text{ \AA}$  at 1.5 m providing of experimental  $q$ -range of  $0.0025 \text{ \AA}^{-1} < q < 0.25 \text{ \AA}^{-1}$ . The neutron wavelength distribution was 0.11. The data were corrected for background, empty beam and converted to absolute

intensity by normalizing by the scattering of 1 mm of hydrogenated water (H<sub>2</sub>O).

Small Angle X-rays Scattering (SAXS) measurements were performed at the ESRF on ID-02 spectrometer and at Soleil on SWING spectrometer. On ID-02, we used the pinhole camera at the energy of 12.46 keV at two sample to detector distances (1m and 10m) corresponding to a  $q$ -range between 0.0008 Å<sup>-1</sup> and 0.3 Å<sup>-1</sup>. The absolute units are obtained by normalizing respect to water (high  $q$ -range) or lupolen (low  $q$ -range) standard. In addition, for some samples, a Bonse-Hart camera setup was used, allowing us to reach  $q$  values lower than 0.0008 Å<sup>-1</sup>. For solutions, SAXS were carried out on SWING beamline and measurements were recorded using 2D AVIEX CCD camera at energy of 7 keV with 2 samples to detector distances: 6.5m and 1.8m, leading to a  $q$ -range lying from 0.0018 Å<sup>-1</sup> to 0.15 Å<sup>-1</sup>.

### 2.3. Transmission electronic microscopy (TEM)

The TEM provides a direct view of silica arrangement in polymer matrix over a wide range of scale from 50 nm to μm. The samples were cut at room temperature by ultramicrotomy using a Leica Ultracut UCT microtome with a diamond knife. The cutting speed was set to 0.2 mm s<sup>-1</sup>. The thin sections of about 40 nm thickness were floated on deionized water and collected on a 400-mesh copper grid. Transmission electron microscopy was performed on a FEI Tecnai F20 ST microscope (field-emission gun operating at 3.8 kV extraction voltage) operating at an accelerating voltage of 200 kV. Precise scans of various regions of the sample were systematically done, starting at a small magnification which was then gradually increased. Then the subsequent analysis of TEM images according to the silica volume fraction is detailed in SI.

### 2.4. Mechanical properties

Mechanical properties have been investigated in the linear regime (low deformation) by coupling Dynamical Mechanical Analysis (DMA) and plate/plate rheology. For DMA experiments rectangular pieces of film 2 cm long × 0.5 cm wide were sanded down to a constant thickness of 0.8 mm. Dynamic mechanical analysis (DMA) measurements were performed on a TA DMA Q800 device in oscillatory tension mode, at fixed deformation rate (0.1%) and fixed frequency (5 Hz), at temperatures ranging from 40 °C to 300 °C with a heating rate of 10 °C/min. Analysis of the oscillatory stress response is done by the software provided by TA; a preloading force of 0.04 N is applied to avoid buckling and ensure complete contact with the plates. We define a reinforcement factor  $E'/E'_0$  as the ratio of the nanocomposites modulus by the reference modulus at  $T/T_\alpha = 1.25$  ( $T_\alpha$  is the main relaxation temperature obtained from DMA measurements).

Oscillatory shear tests (plate/plate rheology), corresponding to low deformation levels (0.5%), were carried out in the dynamic mode in strain-controlled conditions with a plate–plate cell of an ARES spectrometer (Rheometrics-TA) equipped with an air-pulsed oven. This thermal environment ensures a temperature control within 0.1 °C. The samples were placed between the two plates (diameter 1 mm) fixtures at high temperature (160 °C), far above the glass transition, put under slight normal force (around 0.5 N), and temperature was decreased progressively, while gently reducing the gap to maintain a constant low normal force under thermal retraction. The zero gap is set by contact, the error on sample thicknesses is thus minimal; estimated at +0.010 mm with respect to the indicated value. To stay below the limit of linear deformation, the shear amplitude was fixed to 0.5%. Samples are stabilized at the temperature for 30 min before starting measurements. In dynamic mode, the frequency range was from 0.5 to

100 rad/s for different temperatures (from 190 °C to 120 °C), and time-temperature superposition was applied [23].

### 2.5. Extraction experiments

To quantify the weight of bound polymer in the nanocomposites, extraction experiments have been performed as follows. Dry nanocomposites filled with different silica volume fraction were dissolved in good solvent, toluene for PS and DMAc for PMMA, during one day. After that, the solution was centrifugated and the supernatant (excess polymer and excess solvent) was removed. This process is repeated four times to insure well dissolution of all “free chains”. Thermogravimetric analysis (TGA) was then performed on the residual precipitate using a TA TGA Q50 under nitrogen flow to evaluate the quantity of bound polymer in the residual. The sample was heated from 25 to 600 °C at a heating rate of 10 °C/min and weight loss was measured.

### 2.6. DSC measurements

Differential Scanning Calorimetry (DSC) measurements have been performed on TA DSC Q100 under helium flow to measure the glass transition temperature  $T_g$  of the nanocomposites. 5–10 mg of samples was put into a hermetic aluminium pan. Empty cell was used as reference. Samples were heated from 25 °C to 140 °C at a heating rate of 10 °C/min and kept at this temperature during 15 min to erase thermal history of the materials. Then they were cooled to 25 °C with the same speed. This cycle was repeated once and reported  $T_g$  was from the second heating and determined as the mid point of the step in heat flow.

## 3. Results

### 3.1. Native nanoparticles in solution

We first describe the behavior in solution of the different silica beads. Fig. 1 shows the scattering intensity  $I(q)$  obtained by SAXS of the silica solution in DMAc: (a) Nissan-St at 0.25%v/v, (b) Ludox LS at 0.5%v/v and (c) Ludox TM-40 at 0.25%v/v.

All the curves can be described as follows. At high  $q$ , the scattering intensity  $I(q)$  scales as  $q^{-4}$  characteristic of sharp interface between silica surface and solvent. In this  $q$ -range the scattering intensity can be described by a Porod law, which gives the specific surface  $S_{spe}$  of the silica using the relation (1):

$$S_{spe} = I(q)q^4 / (2\pi\Phi_{SiO_2}\Delta\rho^2d) \quad (1)$$

where  $\Phi_{SiO_2}$  is the silica volume fraction,  $\Delta\rho^2 = (\rho_{SiO_2} - \rho_{solvent})^2$  the contrast term between scattering length density of silica and of solvent and  $d$  is the density of the silica (=2.2 g cm<sup>-3</sup>). Table 1 reports the different SLDs and contrast terms in both matrices for the different silica beads.

At intermediate  $q$ , oscillations from the silica form factor, more or less pronounced depending on the polydispersity, are observed. At low  $q$ , we observe a Guinier regime associated to the global size of the silica. For Nissan-St (Fig. 1(a)) a correlation peak appears at very low  $q$  due to repulsive interaction between objects and suggesting a moderate aggregation. The peak positions  $q^*$  give an interparticle distance  $d$  ( $d = (2\pi/q^*)$ ) and an aggregation number  $N_{agg}$  according Equation (2):

$$N_{agg} = (2\pi/q^*)^3 \times (\Phi_{SiO_2}/V_{SiO_2}) \quad (2)$$

where  $\Phi_{SiO_2}$  and  $V_{SiO_2}$  are respectively the volume fraction and volume of silica. One obtains  $N_{agg} = 6$  for Nissan-St indicating that

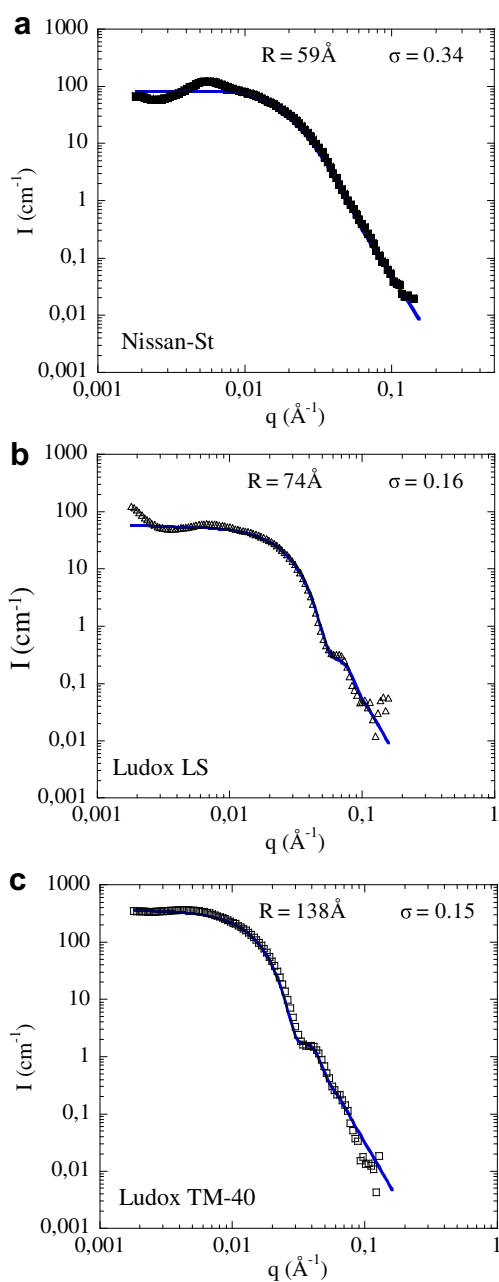


**Fig. 1.** SAXS measurements of two silica beads in solution (DMAc) used in this study: (a) Nissan-St at 0.25%v/v:  $R = 59 \text{ \AA}$  and  $\sigma = 0.34$ , (b) Ludox LS at 0.5%v/v:  $R = 74 \text{ \AA}$  and  $\sigma = 0.16$ , (c) Ludox TM-40 at 0.25%v/v:  $R = 138 \text{ \AA}$  and  $\sigma = 0.15$ . The blue solid lines correspond to the best fit using polydisperse hard sphere form factor. (For interpretation of the references to colour in this figure legend, the reader is referred to the web version of this article.)

the individual objects in this solution are already composed of 6 units of 50 Å. For the following we will consider as primary particle these small assemblies of 6 units. Experimental data can then be well fitted using a polydisperse hard sphere form factor with the mean radius of the silica  $R$  and the polydispersity  $\sigma$  as parameters. Table 2 reports the results obtained for each silica solution.

From the fits we found that Nissan-St have a radius of 59 Å with a large polydispersity of 0.34 and specific surface of 166 m<sup>2</sup>/g. The Ludox LS have slightly greater radius ( $R = 74 \text{ \AA}$ ) but with a lower polydispersity of 0.16 and a specific surface of 202 m<sup>2</sup>/g. The Ludox TM-40 have larger radius: 138 Å with a polydispersity of  $\sigma = 0.15$  and specific surface of 94 m<sup>2</sup>/g. Finally we deduced  $R/R_g$  in PS and

**Table 1**

Density, scattering length density  $\rho$  and contrast terms  $\Delta\rho = (\rho - \rho_{\text{SiO}_2})^2$  from SANS and SAXS of each components used in this study.

| Component        | Density<br>(g cm <sup>-3</sup> ) | $\rho_{\text{SANS}}$<br>( $\times 10^{10}$ cm <sup>-2</sup> ) | $\rho_{\text{SAXS}}$<br>( $\times 10^{10}$ cm <sup>-2</sup> ) | $(\rho - \rho_{\text{SiO}_2})^2$<br>( $\times 10^{20}$ cm <sup>-4</sup> )<br>SAXS/SANS |
|------------------|----------------------------------|---|---|--|
| SiO <sub>2</sub> | 2.2                              | 3.41  | 18.5  | –  |
| DMAc H           | 0.937                            | 0.525   | 8.72  | 95.65/8.32   |
| PS               | 1.04                             | 1.41  | 9.44  | 82.1/4   |
| PMMA             | 1.1                              | 0.99  | 10.05   | 71.4/5.86  |

PMMA and found values always lower than 1, i.e.  $R < R_g$ , suggesting that good dispersion will be insured in nanocomposites [11] (see Table 2).

### 3.2. Silica dispersion in nanocomposites

We now move to silica dispersion in the different polymers. Fig. 2 reports all the SAXS scattering intensities normalized by silica volume fraction  $\Phi_{\text{SiO}_2}$  as a function of scattering wave vector  $q$  for Nissan-St/PMMA (a), Ludox LS/PMMA (b), Ludox LS/PS (c), Ludox TM-40/PMMA (d) and Ludox TM-40/PS (e) nanocomposites. The silica dispersion of Nissan-ST/PS nanocomposites has been detailed elsewhere [20]. For a given silica concentration the scattering curves exhibit similar behavior for all nanocomposites. At high  $q$ , all curves superimpose well suggesting a good normalization by silica volume fraction and scale as  $q^{-4}$  which is characteristic of sharp interface between silica and polymer. At intermediate  $q$ , a shoulder appears whatever the silica and its positions are independent of  $\Phi_{\text{SiO}_2}$ . These shoulders are due to intra-particles structure factor from direct contact between primary particles in larger aggregates [20]. At low  $q$  the overall behaviors depend on silica volume fraction: we observe a plateau at low silica volume fraction and a correlation peak more or less pronounced at large concentration (see below for details). At very low  $q$  an upturn of scattering intensities is measured and clearly observed on unfilled polymers (Fig. 2(a)). Hence we argue that this upturn comes from the presence of crazes created in the matrix during nanocomposites processing. Here we do not discuss the origin of crazes and how the sample process influences them, which are both outside the scope of this paper. Now we will study more precisely the silica dispersion as a function of silica volume fraction  $\Phi_{\text{SiO}_2}$ .

#### 3.2.1. Low $\Phi_{\text{SiO}_2}$ : small fractal aggregates

For low concentration (5%v/v), at low  $q$  (from 0.001 Å<sup>-1</sup> to 0.01 Å<sup>-1</sup>) the scattering intensity scales as  $q^{-D_f}$  and reaches a plateau for the small silica beads suggesting that they arrange in fractal aggregates with a finite size. In this low  $q$ -range data, can be described by a Guinier relation ( $I(q) = I_0 \exp(-q^2 R_g^2/3)$ ) giving the radius of gyration  $R_g$  of the aggregates (not shown here but values are reported in Table 3). For larger particles the Guinier regime is not apparent in the available range. But for both types of particles, the profiles, though different, can also be fitted in the entire  $q$ -range using an aggregate form factor depending on the aggregation number  $N_{\text{agg}}$  (the number of native beads inside the primary aggregate), the fractal dimension of the primary aggregates  $D_f$ , the form factor of a sphere  $P_{\text{native beads}}$  and  $l(R, \sigma)$  the log-normal distribution of the radius (see SI for details). We neglected correlations between aggregates and thus considered in first approximation that the inter-structure factor  $S_{\text{inter-agg}}(q)$  is close to 1. Fig. 3 shows the SAXS scattering intensities for nanocomposites filled with 5%v/v of (a) Nissan-St, (b) Ludox LS and (c) Ludox TM-40 in PS (green squares) and in PMMA (red circles) matrix (the Nissan-St/PS curve comes from reference [20]). In the same figure the best

**Table 2**

Characteristic parameters of Nissan-St, Ludox LS and Ludox TM-40. The values of specific surface are consistent with values given by Sigma Aldrich (190 m<sup>2</sup>/g for Nissan-St, 215 m<sup>2</sup>/g for Ludox LS and 135 m<sup>2</sup>/g for Ludox TM-40).

| Silica      | Radius $R$ (Å) | Polydispersity $\sigma$ | Peak position $q^*$ (Å <sup>-1</sup> ) | Aggregation number $N_{agg}$ | Specific surface $S_{spe}$ (m <sup>2</sup> /g) | $R/R_g^a$ PS/PMMA |
|-------------|----------------|-------------------------|--|------------------------------|--|-------------------|
| Nissan-St   | 59             | 0.34                    | 0.0058                                 | 6                            | 166  | 0.406/0.245       |
| Ludox LS    | 74             | 0.16                    | 0.0068                                 | 2.3                          | 202  | 0.510/0.307       |
| Ludox TM-40 | 138            | 0.15                    | —                                      | —                            | 94   | 0.952/0.573       |

<sup>a</sup>  $R_{gPS} = 0.275(M_w)^{0.5} = 14.5$  nm and  $R_{gPMMA} = 0.041(M_w)^{0.5} = 24.1$  nm.

aggregate fits are shown in solid black line for PS nanocomposites and black dashed line for PMMA nanocomposites. Table 3 reports the corresponding parameters ( $N_{agg}$ ,  $D_f$ ) for all nanocomposites. First, for Nissan-St nanocomposites in PS and PMMA, the curves are very similar: an upturn at very low  $q$  due to crazes (not fitted here)

followed by a Guinier regime at low  $q$ , a shoulder at intermediate  $q$ , to end with a  $q^{-4}$  behavior at high  $q$ . The silica beads organize in small fractal aggregates with  $D_f$  comprised between 1.7 and 1.85. The  $N_{agg}$  is between 3.5 and 10 depending on the matrix. In the intermediate  $q$ -range, a discrepancy between fits and data is

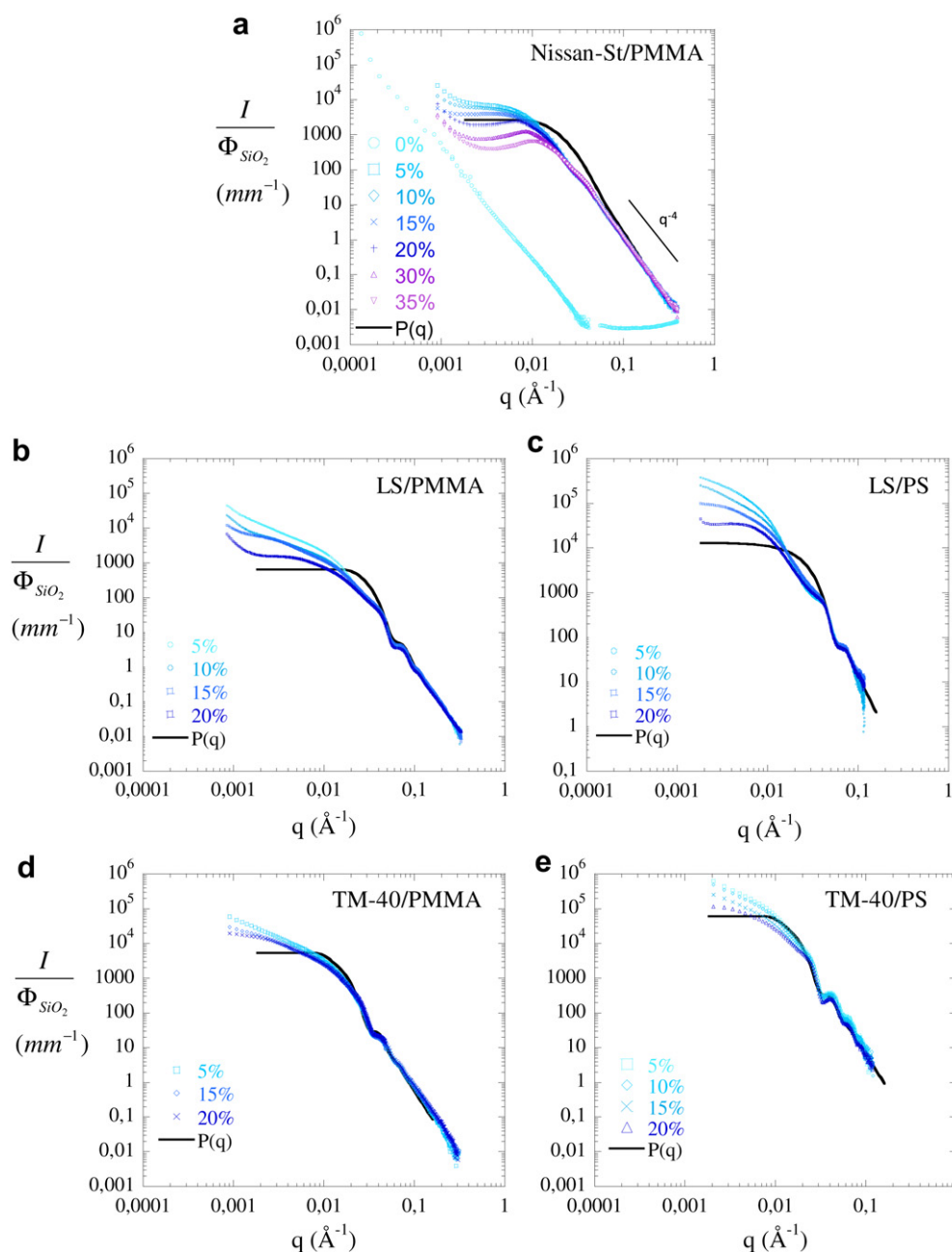


**Fig. 2.** SAXS measurements of Nissan-St/PMMA (a), Ludox LS/PMMA (b), Ludox LS/PS (c), Ludox TM-40/PMMA (d) and Ludox TM-40/PS (e) nanocomposites filled at different silica volume fractions  $\phi_{SiO_2}$ . All curves have been normalized by silica volume fraction  $\phi_{SiO_2}$ . The black solid lines represent the corresponding form factor of the silica native beads. The behavior of Nissan-St/PS nanocomposites (not shown here) has been published previously in reference [20].

**Table 3**  
Structural parameters extracted from aggregates form factor in SAXS and from TEM analysis for the different nanocomposites filled with 5%v/v.

| Silica beads | PS                     |                       |                   | PMMA                   |                       |                   |
|--------------|------------------------|-----------------------|-------------------|------------------------|-----------------------|-------------------|
|              | $R_g$ (nm)<br>SAXS/TEM | $N_{agg}$<br>SAXS/TEM | $D_f$<br>SAXS/TEM | $R_g$ (nm)<br>SAXS/TEM | $N_{agg}$<br>SAXS/TEM | $D_f$<br>SAXS/TEM |
| Nissan-St    | 26/19                  | 10/23                 | 1.85/1.6          | 18.3/20                | 3.5/27                | 1.7/1.6           |
| Ludox LS     | –/–                    | 15/–                  | 2.2/–             | –/22                   | 30/14                 | 1.15/1.6          |
| Ludox TM-40  | –/–                    | 5/–                   | 1.6/–             | –/24                   | 13/3–8 <sup>a</sup>   | 1.1/1.1           |

<sup>a</sup> The sum of two Gaussian functions has been used to reproduce the data (see Fig. 5(c)).

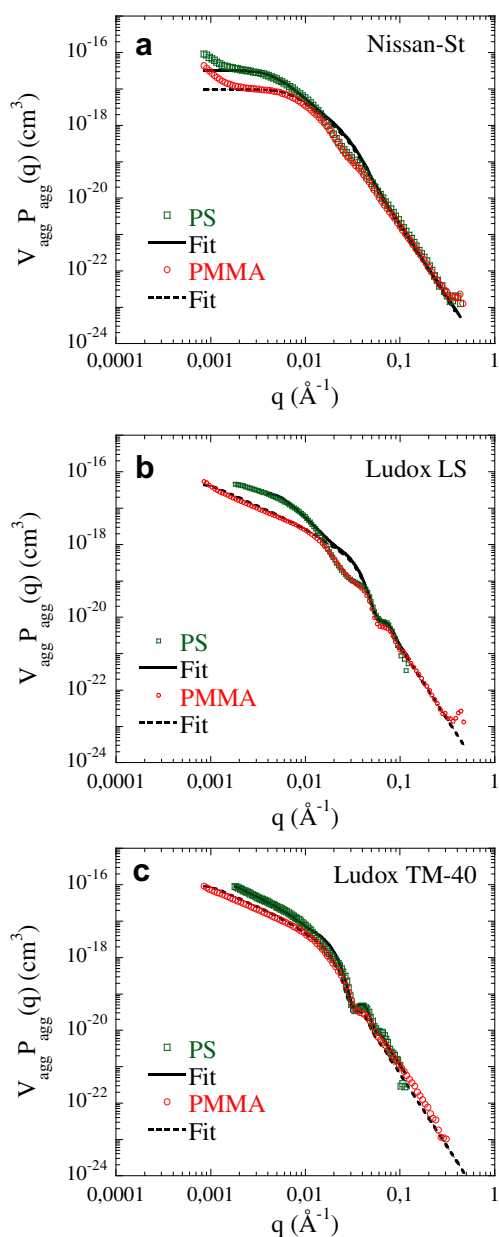


**Fig. 3.** SAXS measurements for nanocomposites filled with 5%v/v of (a) Nissan-St, (b) Ludox LS, (c) Ludox TM-40 in PS matrix (green squares) and in PMMA matrix (red circles). The black solid line and the black dashed line correspond to the best aggregate fits in respectively PS and PMMA matrix. (For interpretation of the references to colour in this figure legend, the reader is referred to the web version of this article.)

observed at the shoulder position corresponding to the inter-particle privilege distance. The correlation hole observed here comes from the convolution of the form factor of the aggregates  $P_{agg}(q)$  with a peak in the intra-structure factor  $S_{intra-agg}(q)$  between primary particles, which is not described in our model. These correlation holes are pronounced for small particles (Nissan-St and Ludox LS) and in PS matrix: interactions between primary particles appear stronger leading to the formation of denser and more homogeneous in size aggregates; the occurrence of this privileged distance is high and the shoulder is thus pronounced. For Ludox TM-40, at intermediate  $q$ -range, the data can be well fitted with the aggregates form factor with  $N_{agg} = 5$  or 13 and  $D_f = 1.6$  or 1.1 for PS or PMMA respectively. Note that, for Ludox LS and Ludox TM-40 systems, the aggregation numbers  $N_{agg}$  are considered as minimal possible values because the Guinier regime at low  $q$  is no longer visible and is certainly matched by the crazes signal. The discrepancy between the data and the fit at very low  $q$  can also be due to the heterogeneous size distribution of the aggregates leading to the absence of clear plateau. Also the inter-particle correlation shoulder is less pronounced suggesting that particles are less packed, but better arranged along linear parts of the aggregates (in particular for PMMA), in agreement with the trend to lower  $D_f$  values.

The silica arrangements in fractal-like aggregates homogeneously dispersed in polymeric matrices are also confirmed on larger scale by TEM images: Nissan-St/PMMA at 5%v/v and Ludox TM-40/PMMA at 5%v/v are reported in Figs. 4 and 5 respectively. We clearly observe that the branches of Nissan-St/PMMA aggregates (Fig. 4) are thick with cross-section containing particles transverse to the branch, while for Ludox TM-40/PMMA (Fig. 5), particles aggregate only in a single row (necklace). This explains the difference in compactness described from SAXS. To be quantitative, TEM images have been analyzed and the structural information on aggregates has been extracted from their projected images using the procedure described in SI. We deduced from this analysis a distribution of aggregation number  $N_{agg}$ , fractal dimension  $D_f$  and radius of gyration  $R_g$  obtained for both PS and PMMA nanocomposites reported in Table 3. First the structural values are consistent with SAXS values with similar  $R_g$  and slight greater  $N_{agg}$  values for TEM (probably because the analysis does not account for polydispersity of the primary particles and is dependent on the thickness of the sample slabs). Second, for Ludox TM-40/PMMA, the TEM analysis reveals the existence of two populations in aggregation numbers ( $N_{agg} = 3$  and 8) suggesting that this system is more heterogeneous in size. We can observe a significant number of single primary particles for TM-40, which are not visible for Nissan-St nanocomposites. In the size distribution we can also point out the existence of few large aggregates (i.e. agglomerates of radius  $R > 80$  nm). These observations well confirm the continuous increase at low  $q$  of the scattering (no plateau). Similar observation is made with LS particles (see Fig. 6(a)) suggesting that smaller size particles (Nissan-St and LS) gives a more homogenous dispersion than the larger ones (TM-40).

### 3.2.2. High $\Phi_{SiO_2}$ : connected silica network

At high  $\Phi_{SiO_2}$ , the scattering intensities (Fig. 2) show a correlation peak at low  $q$ , which is more or less pronounced depending on silica beads. These peaks reveal the apparition of an ordered structure with a characteristic length  $\xi$  ( $\xi = 2\pi/q^*$  with  $q^*$  is the peak position) in the system. At such high concentration, the structure can be described as filler network [20] and can be highlighted by dividing the total scattering intensity by the form factor of the native particles deduced in Fig. 1. The results are presented in Fig. 7 in (a) PMMA matrix and in (b) PS matrix. For Nissan-St nanocomposites there is a well-defined peak whose position scales as  $\Phi^{0.8}$  and  $\Phi^{0.87}$  (for respectively PS and PMMA matrix); this

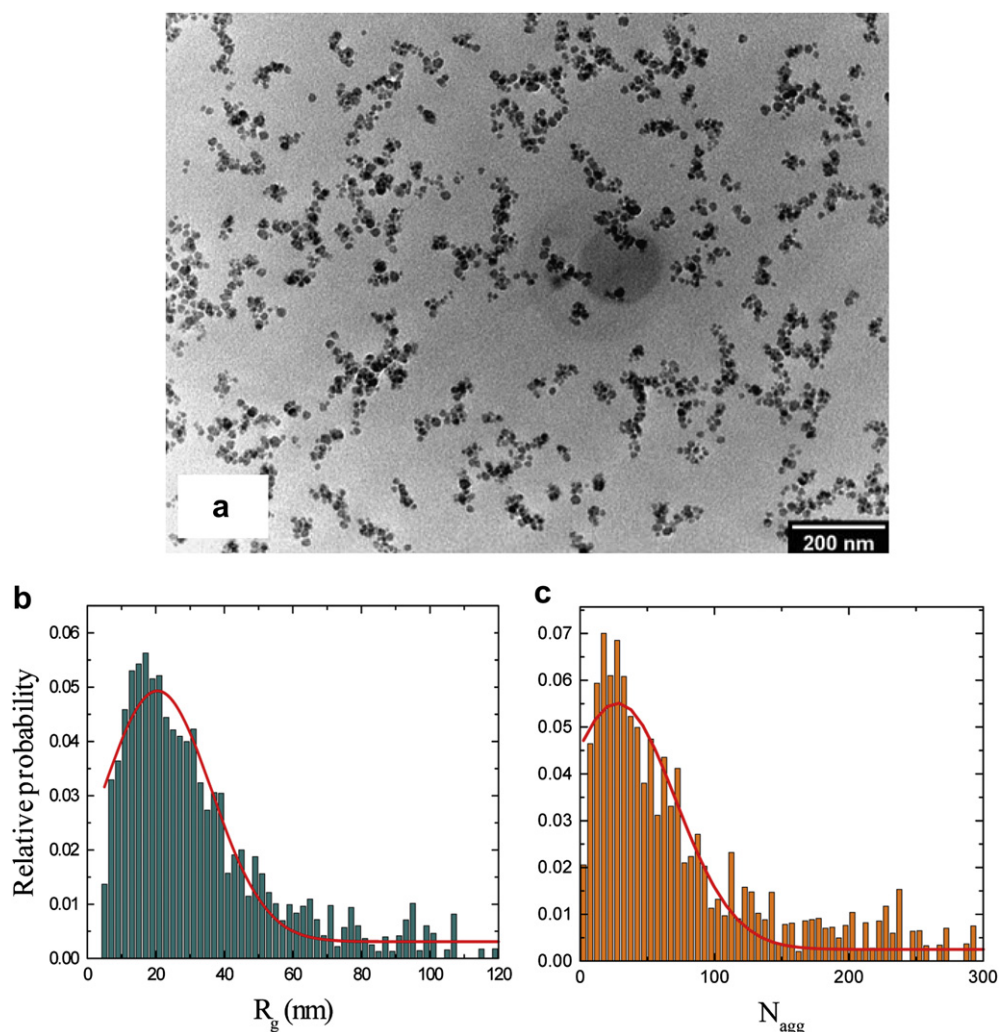


**Fig. 4.** (a) TEM images for 5%v/v Nissan-St/PMMA nanocomposites (scale bar: 200 nm). (b) Radius of gyration  $R_g$  and (c) Aggregation number  $N_{agg}$  obtained by image analysis fitted with a Gaussian distribution. The image at lower magnification is available in SI (Fig. S1).

variation is characteristic of network mesh size evolution when increasing the concentration of the connected strands above percolation threshold [24]. One obtains  $\xi_{PS} = 103$  nm and  $\xi_{PMMA} = 94$  nm at 20%v/v. The peaks are quite broad for Ludox systems. For Ludox TM-40 nanocomposites SAXS curves don't display a visible correlation peak and the scattering signal tend to a plateau indicating the finite size of the structure. The evolution of peak position as a function of the particle size is shown in Fig. 7(c). A linear correlation is found for both polymer matrices indicating that smaller particles give smaller mesh size networks: the rigidity (i.e. the connectivity) of the filler network appears to directly depend on the native particles size.

This description is confirmed by TEM: the network behavior is clearly observed (Fig. 6(b) for Ludox LS and Fig. 8 for Nissan-St and Ludox TM-40) for all nanocomposites. Silica nanoparticles arrange in both polymer matrices to form a connected network with a size of the mesh (or of the holes) consistent with the ones obtained by SAXS. For Ludox TM-40 pictures show also holes, less regularly distributed (in agreement with the weak correlation in SAXS and TEM images analysis) in an apparently connected network. Finally we vary the molecular weight of the polymer matrix, both PS and PMMA, to check its contribution on the particle dispersion. Changing the molecular weights from 100000 to 1000 000 g/mol

appears to have not significant influence on the final filler dispersion (see reference [25] for PS and Fig. S4 in SI for PMMA).

Let us summarize the influence of polymer matrix and particle size on filler dispersion.

Changing the matrix enables the modification of the interaction between polymer and silica and the tuning of the strength of the interfacial interaction (the possible anchoring points may differ from PS to PMMA). The interaction is expected to be weak in PS system (dipole–dipole interaction) whereas it is usually considered stronger in PMMA systems due to possible hydrogen bonds between polymer carbonyl function and silanol group on silica surface [26]. However, our results show that the effect of the polymer on the particle dispersion seems to be relatively limited. At low concentration, the silica native beads arrange in small fractal aggregates dispersed homogeneously in the two polymer matrices. The aggregation number  $N_{agg}$  and fractal dimension  $D_f$  are slightly lower in PMMA nanocomposites than in PS nanocomposites: thus the objects mass is lower and the aggregates more opened in PMMA matrix. At high concentration, silica particles form a connected network whose characteristic size is the mesh size. For a given particle the correlation peaks position  $q^*$  related to mesh size is located at the same  $q$  value whatever the matrix (PS or PMMA).

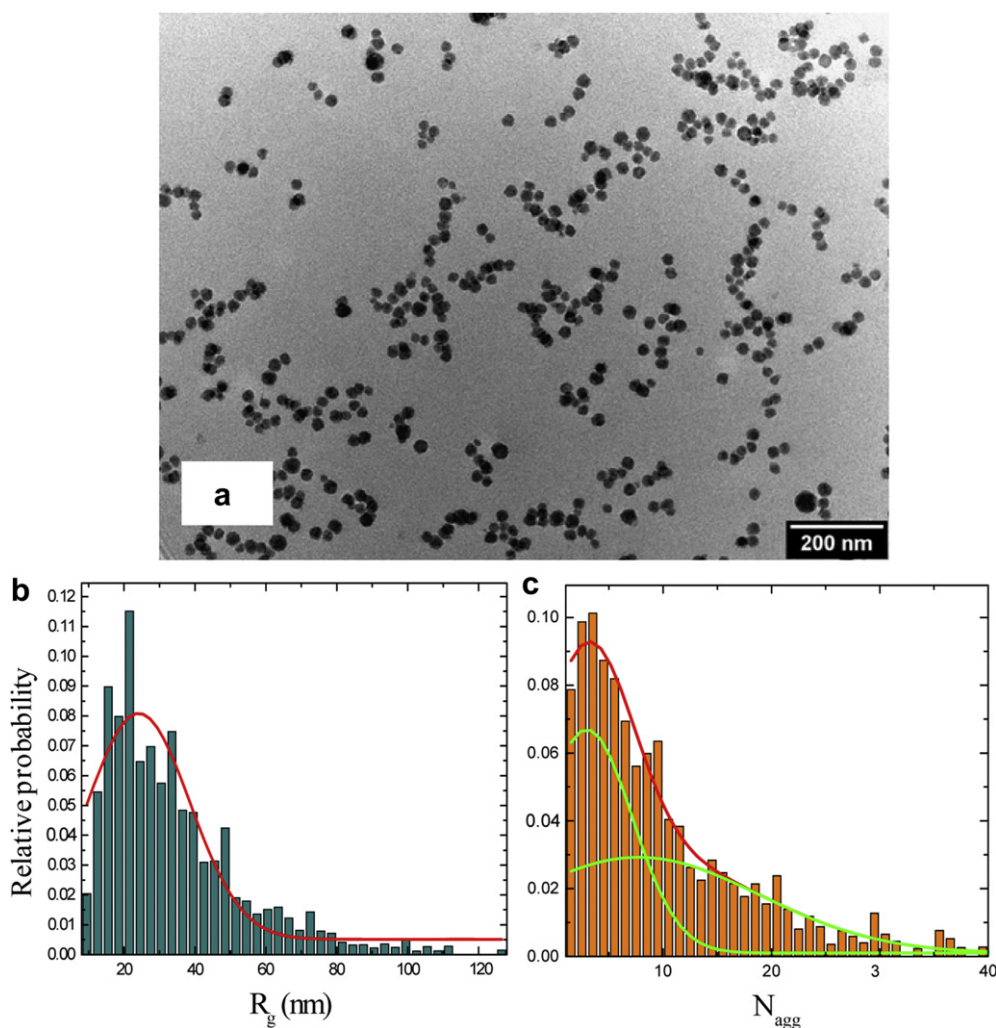


**Fig. 5.** (a) TEM images for 5%v/v Ludox TM-40/PMMA nanocomposites (scale bar: 200 nm). (b) Radius of gyration  $R_g$  and (c) Aggregation number  $N_{agg}$  obtained by image analysis. The sum (red line) of two Gaussians distributions (green line) was used to fit the aggregation number data. The image at lower magnification is available in SI (Fig. S1). (For interpretation of the references to colour in this figure legend, the reader is referred to the web version of this article.)

We now focus on filler size effects on particles dispersion. At low concentration the aggregates appear to be homogeneously distributed for the smaller particle sizes (Nissan-St and Ludox LS) and more heterogeneously for the larger ones (Ludox TM-40). Similarly, for the concentrated regime, the mesh size distribution of the connected filler network is quite narrow for the smaller particles. The peak is not well-defined for the Ludox TM-40 particles and is located at smaller  $q$  value corresponding to a heterogeneous and “swollen” filler network. For Nissan-St and Ludox LS, the filler network is more regular and tight; this is also confirmed by TEM analysis and the size distribution of matrix areas (see Fig. S3 in SI).

### 3.3. Silica aggregation during nanocomposites processing

The identity of the silica dispersion, whatever the beads and the polymer matrix, suggests that samples processing controls the final dispersion state. In this section we will focus on the aggregation process occurring during solvent evaporation. We prepared silica/polymer solutions as described in Experimental part and put it in an oven at 130 °C. Then we sampled at different time: 0 (blue), 1 (green), 2 (red), 2'40 (purple) and 4 (brown) hours for final silica volume fraction of 5%v/v and 0 (blue), 1 (green) and 2'20 (red) hours for final concentration of 20%v/v. For each time we measured

the scattering intensity by SANS and calculated the corresponding silica volume fraction. The scattering intensity is then normalized by the form factor of native particles (determined previously, see Fig. 1(a)) and obtained a structure factor  $S(q)$ .

Fig. 9 shows the corresponding structure factors  $S(q)$  for final silica concentrations of 5%v/v (a) and 20%v/v (b) at different evaporation times. The black squares correspond to the final dispersion in nanocomposites films. At  $t = 0$ , the scattering curves are characterized by a correlation peak giving the mean distance  $d$  between primary particles ( $d = 2\pi/q^*$  with  $q^*$  the peak position). First, when  $t$  increases, the peak position moves to higher  $q$ : the inter-particle distances decrease due to progressive solvent evaporation. Then, for longer  $t$ , the peak position changes and moves to lower  $q$  due to the aggregation of primary particles in small aggregates and thus the distance between them increases. Finally, the peak position and curves remains constant until the end of the processing because a large amount of solvent evaporates and polymer matrix becomes viscous and “freezes” the system in a specific aggregation state. In intermediate  $q$ -range the slope gives the fractal dimension of the forming aggregates ( $D_f = 1.8$ ). We can deduce the aggregation number using Equation (2) at the different times. Table 4 and Table 5 report the different values for respectively 5%v/v and 20%v/v.

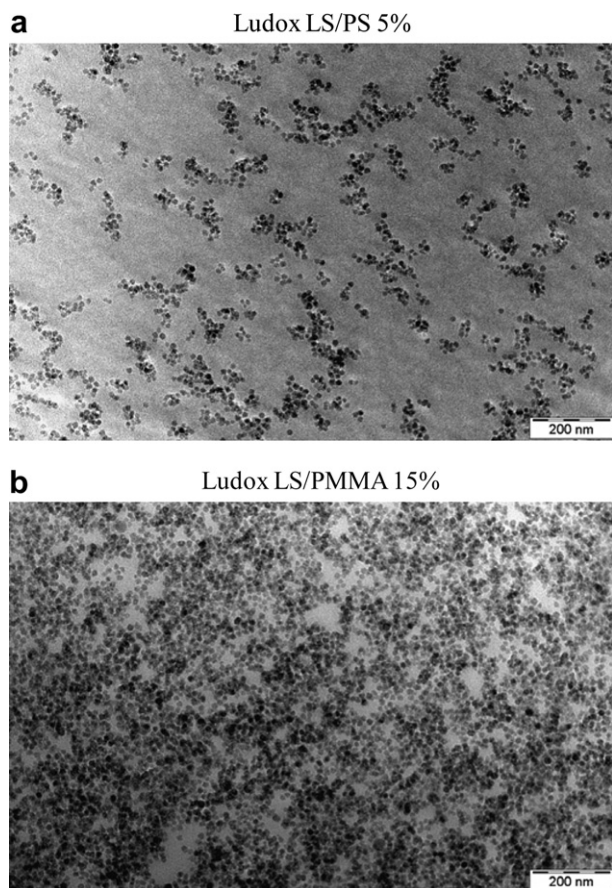


**Fig. 6.** (a) TEM images for 5%v/v Ludox LS/PS nanocomposites (scale bar: 200 nm) and (b) for 15%v/v Ludox LS/PMMA nanocomposites (scale bar: 200 nm).

Before 2 h solutions are still liquid and particles are quite well dispersed ( $N_{agg}$  are comprised between 2 and 3). After 2 h solutions became viscous and particles come close to each other and start to attract via VDW interaction to form small aggregates ( $N_{agg} = 6.2$  for diluted nanocomposite and 3.6 for concentrated nanocomposites). Beyond 2'40 h the peak position moves clearly at low  $q$  and is not available in our  $q$ -range (Fig. 9(a)) suggesting the growth of the aggregates and it became difficult to take sample without influencing the silica dispersion (Fig. 9(b)).

### 3.4. Mechanical properties

In this section the mechanical properties of the nanocomposites will be investigated in the linear regime by coupling DMA and plate/plate rheology.

Fig. 10 shows the evolution of the conservation modulus  $E'$  from DMA as a function of the temperature for PMMA nanocomposites filled with Nissan-St (a) Ludox TM-40 (b) at different silica volume fraction.

For unfilled polymer the DMA curve is classical of amorphous polymer: at low  $T$  (below  $T_{\alpha}$ ), the elastic modulus plateau is around 2500 MPa and corresponds to the glassy regime. When  $T$  increases, a steep decrease is observed and followed by the entanglement rubbery plateau. For higher  $T$  ( $T > 250$  °C), measurements were stopped because the modulus becomes too weak due to the flowing of the samples. When we added silica (Nissan-St (a) or Ludox TM-40 (b)) the curves remain similar at low  $T$ . The main differences occur at higher  $T$  where a mechanical reinforcement effect is clearly observed: the steep decreases are slightly shifted to higher  $T$  and

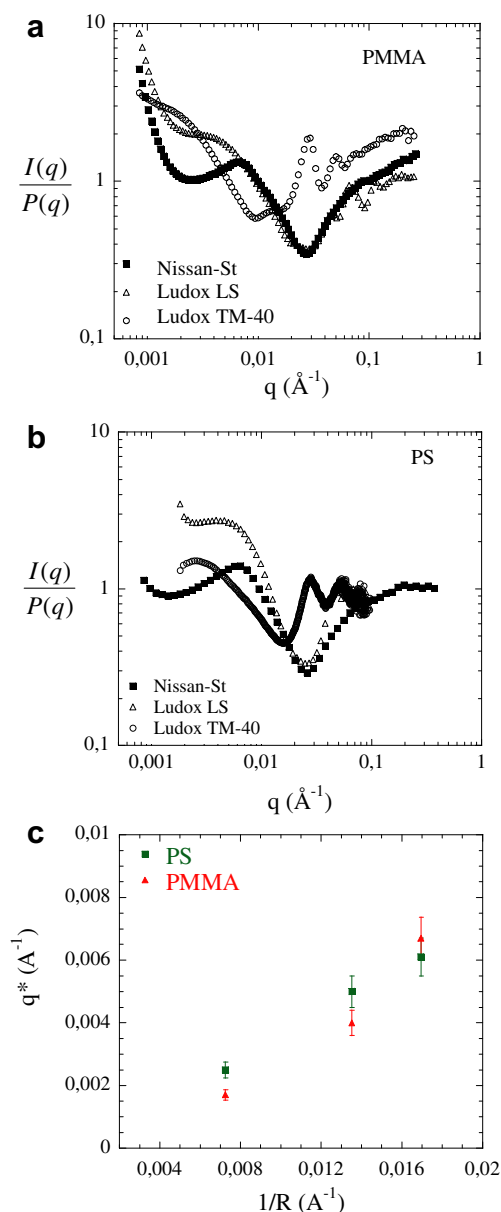


**Fig. 7.** Structure factors obtained by dividing the scattering intensity  $I(q)$  by the form factor  $P(q)$  of native particles for (a) PMMA and (b) PS nanocomposites filled with 20% v/v of Nissan-St (full squares), Ludox LS (open triangles) and Ludox TM-40 (open circles). (c) Evolution of peak position  $q^*$  at 20%v/v as a function of native particle size in both matrices: PS (green squares) and PMMA (red triangles). (For interpretation of the references to colour in this figure legend, the reader is referred to the web version of this article.)

the rubbery plateaus are higher and more pronounced. This effect is emphasized if we followed the evolution of  $E'/E_0$  at  $T/T_{\alpha} = 1.25$  ( $E_0$  is the modulus of the unfilled polymer) as a function of silica volume fraction  $\phi_{SiO_2}$ . Fig. 10(c) presents the comparison of the reinforcement factor for Nissan-St and Ludox TM-40 PMMA nanocomposites. These reinforcement factors present a similar linear behavior at low  $\Phi$  (<5%v/v) followed by a significant deviation from the hydrodynamic behavior when increasing the particles volume fraction. As previously described [20], the appearance of this deviation is related to the filler connectivity threshold, which is observed whatever the nature of the polymer and the particle size. It is interesting to see here that at 20%v/v the levels of the reinforcement factors are stronger for the Nissan particles than for the

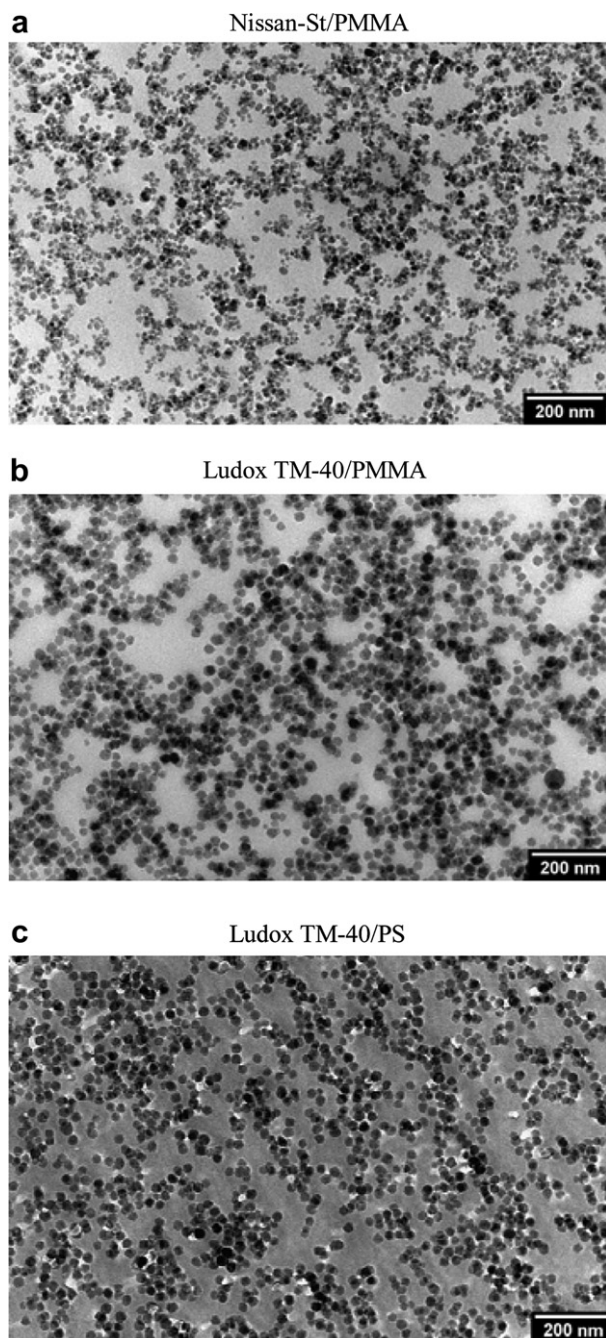


**Fig. 8.** TEM images of nanocomposites filled with 15%v/v for the Nissan-St/PMMA (a), Ludox TM-40/PMMA (b) and Ludox TM-40/PS (c). The scale bar is 200 nm.

Ludox particles (by a factor 2) and also stronger for the PS than for the PMMA matrix (DMA data for PS systems are described in [20]).

Oscillatory shear experiments in the linear viscoelastic regime were also performed to get insight in the reinforcement of nanocomposites and the effect of polymer matrix. Master curves of  $G'$  using WLF time-temperature superposition (TTS) principle [23] are shown in Fig. 11 for Nissan-St/PS (a) and for Nissan-St/PMMA (b). For both unfilled polymers we observed the classical behavior of linear polymer as expected, with slope of  $1/2$  at high frequencies (Rouse relaxation) and slope of 2 at low frequencies in the terminal (flow) regime. For PS and PMMA nanocomposites the TTS principle is also applied with the same shift factors  $a_{T/T_0}$  as for unfilled polymers. At high frequencies no differences are observed, all

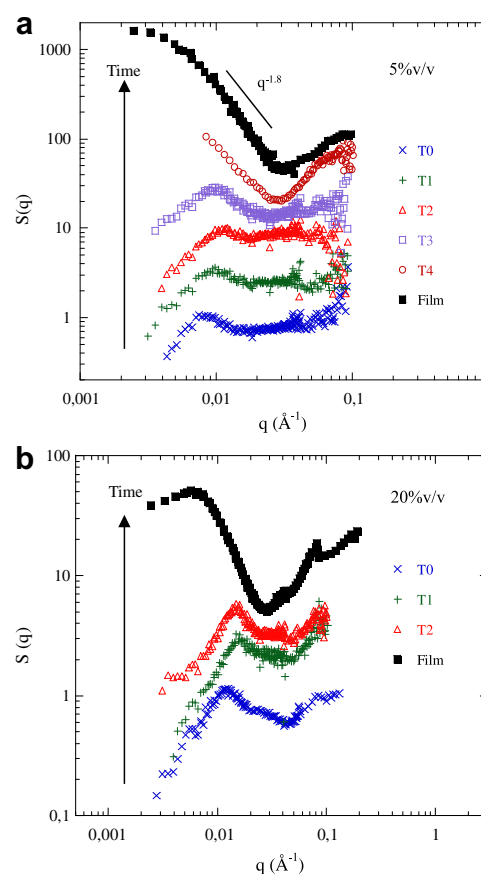


**Fig. 9.** SANS evolution as a function of solvent evaporation time for (a) 5%v/v and (b) 20%v/v Nissan-St/PS nanocomposites. The curves have been shifted for clarity.

curves scale as  $\omega^{1/2}$ . For PS nanocomposites, at intermediate frequencies,  $G'$  increase with silica volume fraction which is correlated to the entanglement mass  $M_e$ . For PMMA, all curves seem to superimpose with the reference one (see Fig. S5 in SI for all silica volume fractions). The largest differences with the unfilled polymers occur at low frequencies when  $G'$  increase and tend to a plateau for PS. The terminal relaxation time  $\tau_{\text{ter}}$  becomes no longer visible in our experimental window. For PMMA the effect is less pronounced but it's clear that there is a slight shift of terminal relaxation time  $\tau_{\text{ter}}$  for 5%v/v revealing the influence of silica on long-range polymer chain motions. These effects on PMMA are similar for Ludox LS nanocomposites (see insert in Fig. 11(b)) and for both PS and PMMA are independent of polymer molecular weight. Fig. 12 presents the results obtained for lower molecular weights ((a) 192 kg/mol for PS and (b) 120 kg/mol for PMMA).

**Table 4**

Silica volume fraction  $\Phi_{\text{SiO}_2}$ , peak position  $q^*$ , aggregation number  $N_{\text{agg}}$  and visual aspect as a function of evaporation time for diluted (5%v/v) Nissan-St/PS nanocomposites.

| Time (hours) | $\Phi_{\text{SiO}_2}$ <sup>a</sup> | $q^*$ ( $\text{\AA}^{-1}$ ) | $N_{\text{agg}}$ <sup>b</sup> | Visual aspect |
|--------------|------------------------------------|-----------------------------|-------------------------------|---------------|
| 0            | 0.005                              | 0.0080                      | 2.9                           | Liquid        |
| 1            | 0.0075                             | 0.0094                      | 2.6                           | Liquid        |
| 2            | 0.013                              | 0.0111                      | 2.7                           | Liquid        |
| 2:40         | 0.02                               | 0.0098                      | 6.2                           | Visquous/Gel  |
| 4            | –                                  | –                           | –                             | Gel           |

<sup>a</sup> The silica volume fraction was determined by measuring the weight of evaporated solvent.

<sup>b</sup> The  $N_{\text{agg}}$  was calculated using Equation (2) with  $R = 59 \text{ \AA}$ .

**Table 5**

Silica volume fraction  $\phi_{\text{SiO}_2}$ , peak position  $q^*$ , aggregation number  $N_{\text{agg}}$  and visual aspect as a function of evaporation time for concentrated (20%v/v) Nissan-St/PS nanocomposites.

| Time (hours) | $\phi_{\text{SiO}_2}$ | $q^*$  | $N_{\text{agg}}$ | Visual aspect |
|--------------|-----------------------|--------|------------------|---------------|
| 0            | 0.02                  | 0.0120 | 3.3              | Liquid        |
| 1            | 0.028                 | 0.0156 | 2.1              | Liquid        |
| 2'20         | 0.039                 | 0.0146 | 3.6              | Visquous/Gel  |

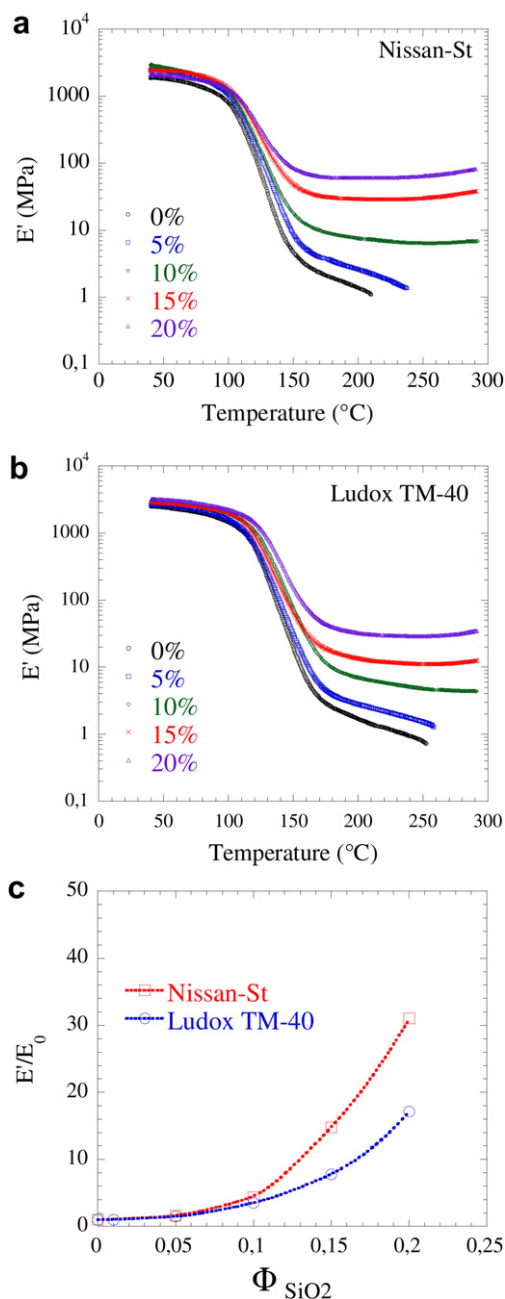


**Fig. 10.** DMA measurements of conservation modulus  $E'$  as a function of temperature for Nissan-St/PMMA (a) and Ludox TM-40/PMMA (b) nanocomposites at different silica volume fraction. (c) Reinforcement factor  $E'/E_0$  as a function of silica volume fractions at  $T/T_\alpha = 1.25$  for Nissan-St (red squares) and Ludox TM-40 (blue circles) PMMA nanocomposites. (For interpretation of the references to colour in this figure legend, the reader is referred to the web version of this article.)

#### 4. Discussion

Nowadays, the better understanding of the correlation between the local organization of the nanoparticles inside the polymer matrix and the macroscopic mechanical and rheological behavior of the materials is still a challenge. It remains difficult to understand it mainly because these correlations are mostly system dependent due to specific interactions and thus difficult to translate into general behaviors. On the basis of a previous study [20] on silica/PS model nanocomposites we here investigate the role of various significant parameters of the system (the particle size, the molecular weight and the nature of polymer matrix) on the local particle dispersion and its direct influence on the mechanical properties. While keeping unchanged the nanocomposites processing conditions, we studied three sizes of silica particles and two different polymer matrices with similar  $T_g$  ( $\sim 100$  °C) and molecular weights but with also different interaction potentials with silica. The first important point is that, whatever the systems, a structural transition is observed from non-connected fractal aggregates at low silica volume fraction to connected network above the percolation threshold  $\Phi_c$ , confirmed both by SAXS measurements and TEM pictures. Second, our silica arrangements differ from the ones commonly observed in the literature for PS [18,19] or PMMA [27] nanocomposites. Changes in filler size or polymer matrix do not induce drastic modifications on silica structures and thus on mechanical reinforcement suggesting that preparation conditions governed the general behavior of nanocomposites: the filler

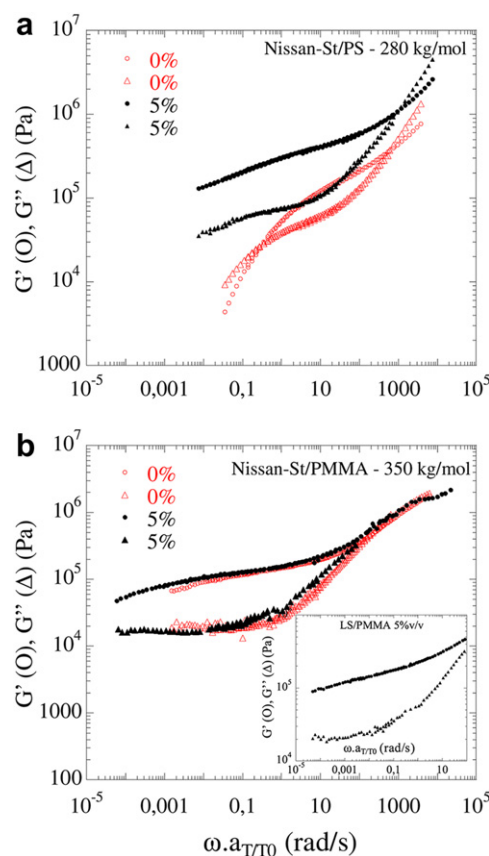


**Fig. 11.** Oscillatory shear experiments for (a) Nissan-St/PS and (b) Nissan-St/PMMA with in insert the mechanical behavior of 5%v/v Ludox LS/PMMA nanocomposite. Master curves of  $G'$  and  $G''$  are obtained using TTS principle with a reference temperature of 143 °C. The parameters of the TTS are  $C_1 = 6.72$  and  $C_2 = 98$  °C for PS (see the reference [20] for details),  $C_1 = 11$  and  $C_2 = 120$  °C for PMMA [23].

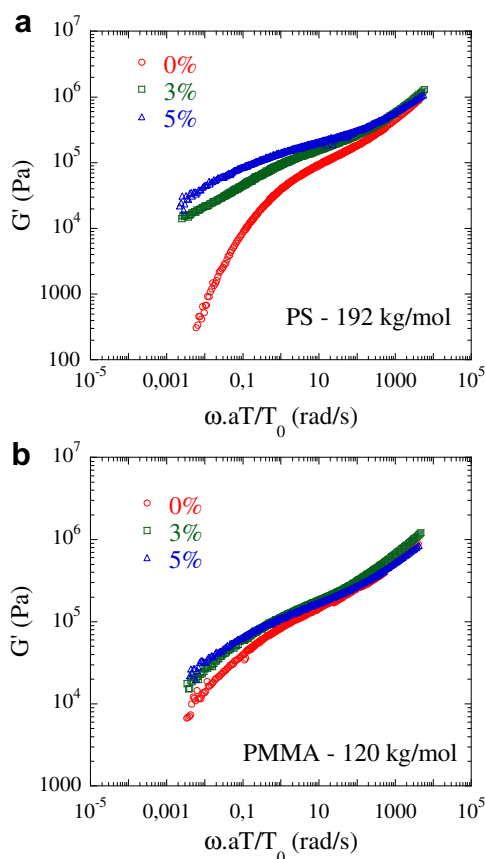


Fig. 12. Oscillatory shear experiments for Nissan-St/PS 192 kg/mol (a) and Nissan-St/PMMA 120 kg/mol (b) at 0%, 3% and 5%v/v.

dispersion is very dependent on the mixing procedure used for nanocomposites preparation [28] and the aggregation mechanisms depend on processing and solvent used [18]. We followed by SANS the evolution of silica aggregation during processing. The aggregation is close to DLCA process and the aggregation state appears frozen when sample becomes viscous. Therefore the solvent evaporation makes it more and more viscous and is sufficiently quick to freeze the aggregation in a well dispersed state (i.e. aggregates with low  $N_{agg}$ ) at all scales. At the same time, the mechanical measurements clearly show a modification of the reinforcement above  $T_g$ . At large particle volume fractions we observe a fast increase of modulus and at low concentrations the increase of terminal time (observed at low frequencies) is akin to a solid-like behavior. Such observations have been discussed previously on Nissan-St/PS nanocomposites [20]: we argued that at high concentration the filler/filler interaction is the dominant mechanism responsible of the high reinforcement (filler connected network regime) and, at low concentration, long-range effects in polymer matrix need to be considered to explain the increase of times and solid-like. We will now detail our results as a function of silica organization, polymer matrix and filler size.

#### 4.1. Filler connectivity and strong mechanical reinforcement at high $\Phi_{SiO_2}$

A structural modification is clearly observed with the increase in volume fraction of nanoparticles, which simultaneously arrange in a connected network: the characteristic size is thus the mesh size and is accessible by SAXS through the peak position  $q^*$  (this is also

confirmed by TEM images). We assume that the formation of this network is close to a percolation mechanism of former small aggregates [24]. Ludox beads show larger mesh sizes distribution as shown in Fig. 7 with a broad peak for Ludox TM-40 compared to narrow peak of Nissan-St and we observe a linear correlation between the mesh size of the filler network and the native particle radius (Fig. 7(c)). There is a direct correlation between filler network appearance and increase of mechanical modulus: it is more pronounced for higher connectivity (as observed for smaller particles in both matrices). We directly see that filler contacts in the network make possible the stress transfer leading to an increase of reinforcement and thermo-mechanical stability (observed in DMA). It is clear that the classical reinforcement model based on hydrodynamic effects cannot describe such strong increase. Similar observations have been previously presented in the literature and formerly described in terms of percolation for fillers with high aspect ratio [5,29,30]. In the case of aggregates of spherical particles, attractive predictions have been proposed to also take into account the percolation effects [5]: above the percolation threshold the reinforcement factor should scale as  $\phi^{2/(3-D_f)}$ . Unfortunately they cannot describe our experimental data without introducing unrealistic parameters with respect to our structural investigations (we have to remember that our aggregates remain small, so that their fractal nature remains limited).

Another interesting point is the correlation between the filler size and the amplitude of the reinforcement (Fig. 10(c)). It can be directly correlated with the strength of the filler network. Larger particles lead to lower reinforcement since the surface of contacts between aggregates decreases when the size increases, so that the efficiency of connectivity decreases. As the reinforcement is related to filler connectivity in this range of silica concentration, this leads to a decrease of the reinforcement: the filler rigidity depends on the inter-particle attractive interaction. The nature of the interface between fillers and polymer has also been recently modified by grafting PS chains onto the Nissan-St silica surface. The grafting process doesn't affect the silica dispersion (compared to the ungrafted case) but mechanical reinforcement is clearly lower. A similar conclusion is proposed: in these grafted systems the grafted chains squeezed between two particles reduce the rigidity of the filler network [31].

The second effect is the influence of the polymer: for a given particle a strong variation of the reinforcement amplitude between PS (see in reference [20]) and PMMA is observed. The experimental threshold in silica concentration (increase of  $E'/E_0$ ) is larger for PMMA than for PS nanocomposites. It remains however correlated to the formation of silica network: the evolution of peak position in SAXS scales as  $\Phi^{0.8}$ , as expected above the percolation threshold and TEM images confirm such behavior. This moderate reinforcement in PMMA can be explained first through the structure by the smaller aggregates size and fractal dimension which shift the percolation threshold at higher  $\Phi$  and second by the difference of PMMA pure polymer behavior which exhibits longer entanglement rubbery plateau (more extended to lower pulsations); this makes  $E_0$  larger at the temperature used for this determination and naturally decrease the ratio  $E'/E_0$ . Not accounting for  $E_0$  and considering directly the modulus  $E'$ , we see that the values for PS and PMMA are very close (for high silica concentrations) suggesting that  $E'$  of the nanocomposites would be dominated by the filler network contribution, irrespectively of the pure polymer rheology [32].

#### 4.2. Indirect connectivity and solid-like behavior at low $\Phi_{SiO_2}$

At low concentration, silica beads arrange in non-connected fractal aggregates dispersed in both polymer matrices. The particles organization inside the polymer matrix does not depend on the

nature and of the molecular weights of the polymer. However, the homogeneity of the dispersion depends on the size of the particle. SAXS measurements and TEM images show that the dispersion is more homogenous for the smaller particles (Nissan-St and Ludox LS) than for the larger ones (Ludox TM-40). As explained above, during the solvent evaporation process, native particles form aggregates with sizes remaining unchanged (i.e. aggregation state is “frozen”) when the viscosity of the medium increases and thus prevents the diffusion of the particles. It also indicates that the kinetic of aggregation process is faster for the small particles (due to Van der Waals attraction and/or faster diffusion coefficients) than for the large ones. The formation of small aggregates is completed for the small particles at the frozen step and not for the larger one, illustrating the observed differences in size heterogeneity at the final state. The mechanical properties show a large increase of terminal times akin to a solid-like behavior for  $G'(\omega)$ , and a constant modulus at high temperature for DMA: this suggests that, whatever the polymer matrix or silica beads, we are close to gel point with percolation behavior: the latter, different from direct filler connectivity, would occur through the polymer matrix and has been reported in other systems [33–35]. Recently the different origins of such reinforcement have been invoked by different authors in the literature [20,36,37]: (i) filler effects, (ii) glassy layers or glassy paths, (iii) bridging effects or chain confinement, (iv) aggregates diffusion or pre-transitional network effects, (v) long-range effects in polymer matrix.

#### 4.2.1. Filler effects

First the enhancement of mechanical properties at intermediate pulsation  $\omega$  (in the entanglement plateau) can be explained by the filler effects only related to silica volume fraction  $\Phi$ . Using the Guth and Smallwood equation ( $G'/G'_0 = 1 + 2.5\Phi + 14\Phi^2$ , note that the aspect ratios of aggregates are close to 1) the modulus of the nanocomposites can be predicted for spherical spheres. Fig. 13 shows the comparison between experimental data and the theoretical predictions for Nissan-St/PS (squares) and Nissan-St/PMMA (circles) nanocomposites at different molecular weights. For Nissan-St/PS nanocomposites the theory does not reproduce our data. This deviation (lower for lower molecular weight) could arise from modifications of chain dynamics and/or increase of entanglement density, which are not considered in the Guth and Smallwood equation and will be discussed below. For Nissan-St/PMMA

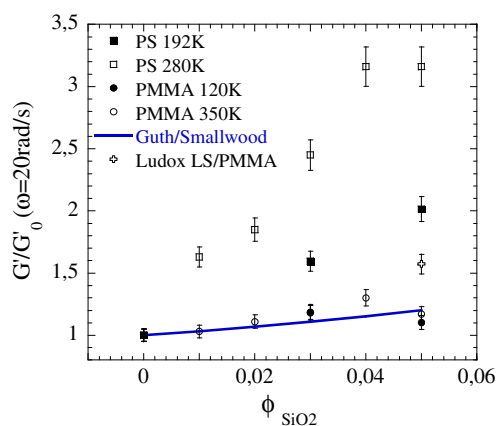


**Fig. 13.** Comparison at  $\omega = 20$  rad/s between theoretical predictions of Guth/Smallwood (blue continuous line) and experimental data for Nissan-St/PS (squares, full: 192 kg/mol, empty: 280 kg/mol) and Nissan-St/PMMA (circles, full: 120 kg/mol, empty: 350 kg/mol) nanocomposites. We also put for comparison the 5%v/v Ludox LS/PMMA nanocomposites (open cross). (For interpretation of the references to colour in this figure legend, the reader is referred to the web version of this article.)

nanocomposites this deviation is not observed illustrating that, in this case, our observations are consistent with the filler effect interpretation.

To improve the fit to experimental data one can take  $\Phi$  as adjustable parameter, representative of the effective volume fraction, which is the sum of silica volume fraction and bound polymer volume fraction. The existence of bound polymer has been proposed to explain the deviation from the hydrodynamic reinforcement. To investigate this point we performed extraction experiments to measure the quantity of bound polymer on our samples. Fig. 14 reports the results. For Nissan-St/PS nanocomposites (at 280 kg/mol) we obtained 0.28 mg/mg of mass of bound polymer per mass of silica, independently of silica volume fraction. For Nissan-St/PMMA (at 350 kg/mol) no bound polymer is found for silica volume fraction lower than 7.5%v/v (consistent with the fact that the reinforcement can be explained by the filler effect in this range of concentration), and a value around 0.11 mg/mg for larger concentrations. These values suggest that both PS and PMMA adsorb on silica surface, with a higher effect for PS at all concentrations, which was not expected. However, first we must keep in mind the known dependence of these results on experimental setup (solvent used, number of washes), and second the quantity of bound polymer is always low. To appreciate this, the mass ratio can be converted to a bound polymer/silica volume ratio  $\Phi_{\text{bound}}$ . Assuming this bound chains form rigid phase around filler, we can define an effective volume fraction  $\Phi_{\text{eff}}$  defined as  $\Phi_{\text{eff}} = \Phi_{\text{SiO}_2} (1 + \Phi_{\text{bound}})$ . One can then replace  $\Phi_{\text{SiO}_2}$  by  $\Phi_{\text{eff}}$  in Guth and Smallwood equation. In practice value of  $\Phi_{\text{bound}}$  is too low to reproduce our data for PS. Thus a coupling of the filler effect with bound polymer is thus not sufficient to explain our reinforcement.

#### 4.2.2. Chain dynamics

A second possible origin is a modification of local segmental dynamic by the presence of silica. At low  $\omega$  the additional elastic contribution can be explained by the existence of interaction between polymer chains and particles leading to a reduction of polymer mobility or, in an extreme case, to the formation of glassy layers around aggregates increasing the rigid phase volume fraction, or glassy paths creating filler/polymer/filler network [9,16]. The effect of fillers on glass transition temperature is still unclear since various works reported contradictory results depending on filler dispersion, polymer/filler interaction and processing conditions [38,39]. One way to investigate the presence or absence of glassy regions is to perform calorimetric measurements [38,40]. We performed heat capacities measurements for Nissan-St/PS and

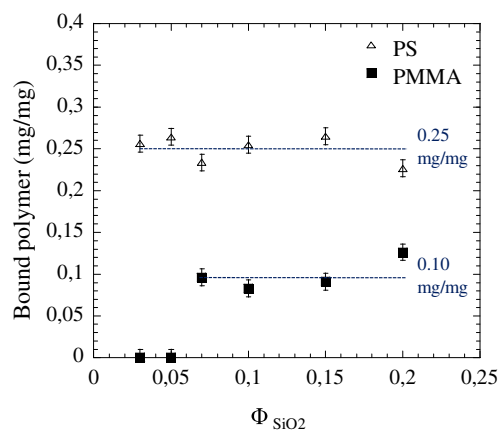


**Fig. 14.** Mass of polymer from extraction experiments as a function of silica volume fractions: PS (empty triangles), PMMA (full squares). The dash lines are guide for eyes.

Nissan-St/PMMA nanocomposites as a function of silica volume fraction as shown in Fig. 15. The evolution of  $\Delta C_p$  can be described by considering that the entire polymer participate to the glass transition as  $\Delta C_p = [\Delta C_{p0}(1-\Phi)\rho_{\text{polymer}}]/[\Phi\rho_{\text{SiO}_2}+(1-\Phi)\rho_{\text{polymer}}]$ ; this gives the blue continuous line on Fig. 15 and well fits our data.  $\Delta C_p$  decreases when filler volume fraction increases: this suggests that filler does not contribute to the glass transition. Moreover, in this concentration range (<5%v/v) there is also no significant change in  $T_g$ :  $\Delta T_g$  (PS) = +1 °C [20] and  $\Delta T_g$  (PMMA) = +1 °C (see Fig. S6 for the evolution of  $T_g$  as a function of silica volume fraction for all nanocomposites). Note also that, as reported above, the oscillatory shear measurements well obey to the time-temperature superposition (TTS) with the same parameters as for the pure matrix. Thus our results show no macroscopic evidence of immobilized polymer or drastic suppression of polymer mobility whatever the polymer matrix or the polymer size.

We recall here that we also addressed formerly such hypothesis of immobilized polymer or glassy layers in our Nissan-St/PS nanocomposites through SANS measurements on stretched samples [41]. Chain conformation has been measured under deformation and compared to the reference one (without silica). No changes have been observed and we concluded that, if glassy regions exist, they concern a very small amount of chains. These experiments concern a much higher deformation range (elongation ratio from 1.2 to 6) but the stress was still noticeably higher than the one of pure matrix. One could expect the same results for PMMA systems as the filler structure and mechanical reinforcement are very close. We can suppose that PMMA chain conformation remains also unchanged.

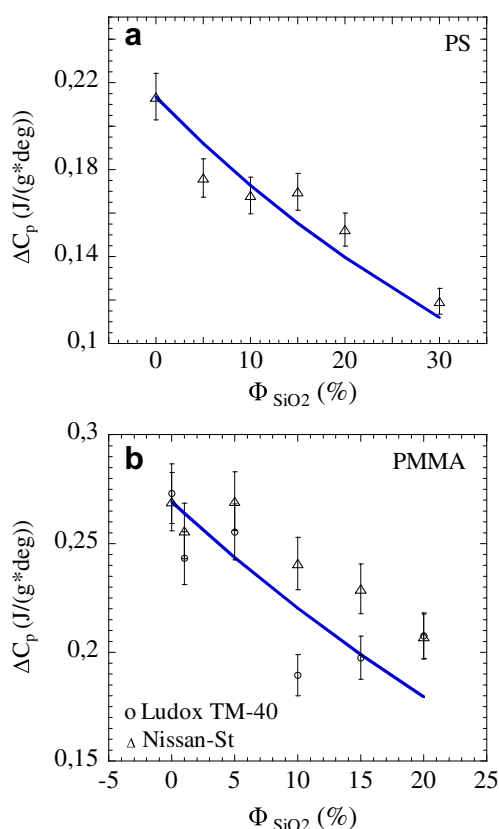


**Fig. 15.** Difference in heat capacity at the glass transition temperature  $T_g$  for Nissan-St/PS (a) and PMMA nanocomposites (b). For PMMA we plot the results for Ludox TM-40 (circles) and Nissan-St (triangles) silica beads. The continuous line represents the reduction of  $\Delta C_p$  if the entire polymer participates to the glass transition.

A third origin of the increase of low deformation modulus in this concentration range can be due to chain bridging [42] between aggregates. This assumption implies in our case that the radius of gyration of the chains involved would be increased, since they would have to join two aggregates separated in average by distances substantially larger than the  $R_g$  at rest. Here again this is not evidenced by SANS: on Nissan-St/PS at rest the form factor of a single chain remains unchanged. We do not observe any differences between filled and unfilled polymers: it does not affect the global chain conformation [25]: chain bridging would also concern a small amount of chains. Finally, the modification of the nature of the interface between fillers and polymer by grafting PS chains [31] does not affect either the silica dispersion (similar to the ungrafted systems) or the mechanical response at low  $\Phi$  <5%v/v. The solid-like behavior is still observed in this grafted case, while the polymer/filler interaction should be modified. This suggests that the reinforcement in our model nanocomposites leading to the existence of long relaxation time is not only the result of specific polymer/filler interaction.

#### 4.2.3. Alternative origins of the observed reinforcement

The above discussion rules out several possible origins for the viscoelastic behavior at low concentration for PS, which remains to explain. What is remarkable is that not only the characteristic times are increased (“horizontal stretching” at low pulsation) but also the modulus takes larger value over the whole time range covered by the pure polymer (apparent vertical shift parallel to the modulus axis). This “horizontal stretching” could be attributed to the slowing down of chain reptation close to the filler surface due to transient chain immobilization around particles [43]. This is equivalent to the increase of a friction coefficient  $\xi$  (as  $\tau_{\text{ter}}$  scales as  $\xi/kT$ ), or close to the sticky reptation [42,44,45]. However a simple increase of  $\xi$  cannot explain the “vertical shift”, which could be attributed to an increase in polymer entanglement due to segmental packing created by the presence of silica (and responsible of measured bound (adsorbed) polymer [45]). Recently, simulations [46], assuming no particle–polymer interaction in reinforced elastomers, reveal that reinforcement results from the increase in chain entanglement density around particles. These interpretations, independent of silica dispersion, support our experimental results on Nissan-St/PS nanocomposites and previous observations of the literature [47,48].

For PMMA nanocomposites, while the structural dispersion and the mechanical properties appear similar, the origins of reinforcement may be different. The reinforcement appears less pronounced: the increase of the modulus at high concentration is moderate and the increase of  $G_0$  in intermediate  $\omega$  (vertical shift) can be simply explained by a classical filler effect (Fig. 13) suggesting that entanglements density is not affected in that case. The increase of the longest terminal time  $\tau_{\text{ter}}$  (“horizontal stretching”) can here be related to the increase of friction coefficient  $\xi$ . The interaction between ester groups of PMMA and silanol groups of silica surface may lead to preferential adsorption that reduces the chain backbone motions [49] and the ability of the polymer to reptate. The disentanglement time should be increased by the presence of nanoparticles and could explain the increase of the long relaxation time in these systems. This effect could concern a small fraction of chains and could explain the absence of bound polymer measured in PMMA nanocomposites.

## 5. Conclusion

Model silica nanocomposites were prepared by solvent evaporation method and the effects of polymer matrix (PS or PMMA) and particles size have been studied on silica dispersion and mechanical

properties. The silica dispersion at different length scales has been investigated by coupling SAXS measurements and TEM images. A first clear result is that at low volume fraction silica particles arrange in small fractal aggregates, for both particle sizes, and that at same size these aggregates are very similar for both polymers. A second general result is that at high volume fraction silica forms a connected network through the matrix, which increases considerably the reinforcement. The strength of the connectivity, tunable by the particles size and characterized owing to structural studies, modulates the strength of the reinforcement. A third common result is that nanocomposites exhibit long terminal times and even a solid-like behavior. But this third effect occurs in a different way for the two polymers. For PMMA we only observe an increase in terminal times. For PS, we recover previous observations on large set of particle size and molecular weight: slower relaxation at long times lead to higher value of the modulus, but the modulus is also increased over the whole time range covered by the pure polymer. In connection with other results on the same systems we rule out several origins proposed for this effect (glassy interfacial dynamics, bridging). These differences between PS and PMMA can be related to the nature of the interaction between silica particles and polymers. The observed increase of both plateau modulus and time range effects could be attributed to increase in chain entanglements density for PS, while for PMMA an increase of chain friction due to transient immobilization around particles is sufficient to explain the time shift. More studies on PMMA or on other different polymers must be conducted to get a comprehensive view of the different systems.

### Acknowledgment

Commissariat à l'Energie Atomique (CEA) and Région Bretagne are acknowledged for financial support. The authors thank the European Synchrotron Radiation Facility (ERSF, Grenoble, France) and SOLEIL synchrotron (Saint-Aubin, France) for beam time allocation and Florian Meneau (SWING, Soleil) and Emanuela Di Cola (ID-02, ESRF) for their help during the experiments. Sylvère Said is also acknowledged for fruitful discussion.

### Appendix. Supplementary material

Supplementary material associated with this article can be found, in the online version, at [doi:10.1016/j.polymer.2011.12.001](https://doi.org/10.1016/j.polymer.2011.12.001).

### References

- [1] Paul DR, Robeson LM. *Polymer* 2008;49:3187–204.
- [2] Krishnamoorti R, Vaia RA. *J Polym Sci Part B Polym Phys* 2007;45:3252–6.
- [3] Jancar J, Douglas JF, Starr FW, Kumar SK, Cassagnau P, Lesser AJ, et al. *Polymer* 2010;51:3321–43.
- [4] Ganesan V, Ellison CJ, Pryamitsyn V. *Soft Matter* 2010;6:4010–25.
- [5] Heinrich G, Kluppel M, Vilgis TA. *Curr Opin Solid State Mater Sci* 2002;6:195–203.
- [6] Witten TA, Rubinstein M, Colby RH. *Journal de Physique II*; 3: 367–383.
- [7] Dutta NK, Choudhury NR, Haidar B, Vidal A, Donnet JB, Delmotte L, et al. *Polymer* 1994;35:4293–9.
- [8] Berriot J, Martin F, Montes H, Monnerie L, Sotta P. *Polymer* 2003;44:1437–47.
- [9] Berriot J, Montes H, Lequeux F, Long D, Sotta P. *Macromolecules* 2002;35:9756–62.
- [10] Long L, Lequeux F. *Eur Phys J E* 2001;4:371.
- [11] Mackay ME, Tuteja A, Duxbury PM, Hawker CJ, Van Horn B, Guan Z, et al. *Science* 2006;311:1740–3.
- [12] (a) Chevigny C, Dalmas F, Di Cola E, Gignes D, Bertin D, Boué F, et al. *Macromolecules* 2011;44:122–3;  
(b) Chevigny C, Jestin J, Gignes D, Schweins R, Di Cola E, Dalmas F, et al. *Macromolecules* 2010;43:4833–7.
- [13] Radhakrishnan B, Ranjan R, Brittain WJ. *Soft Matter* 2006;2:386–96.
- [14] Balazs AC, Emrick T, Russell TP. *Science* 2006;314:1107–10.
- [15] Akcora P, Hongjun L, Kumar SK, Moll J, Li Y, Benicewicz BC, et al. *Nat Mater* 2009;8:354–9.
- [16] Akcora P, Kumar SK, Moll J, Lewis S, Schadler LS, Li Y, et al. *Macromolecules* 2010;43:1003–10.
- [17] Jordan J, Jacob KI, Tannenbaum R, Sharaf MA, Jasiuk I. *Mater Sci Eng A* 2005;393:1–11.
- [18] Sen S, Xie Y, Bansal A, Yang H, Cho K, Schadler LS, et al. *Eur Phys J* 2007;141:161–5. *Special Topics*.
- [19] Bansal A, Yang H, Li C, Cho K, Benicewicz BC, Kumar SK, et al. *Nat Mater* 2005;4:693.
- [20] Jouault N, Vallat P, Dalmas F, Said S, Jestin J, Boué F. *Macromolecules* 2009;42:2031–3040.
- [21] Tannenbaum R, Zubris M, David K, Ciprari D, Jacob K, Jasiuk I, et al. *Phys Chem B* 2006;110:2227–32.
- [22] Ciprari D, Jacob K, Tannenbaum R. *Macromolecules* 2006;39:6565–73.
- [23] Williams ML, Landel RF, Ferry JD. *J Am Chem Soc* 1955;77:3701.
- [24] Stauffer D. *Introduction to percolation theory*. Taylor and Francis; 1985.
- [25] Jouault N, Dalmas F, Said S, Di Cola E, Schweins R, Jestin J, et al. *Macromolecules* 2010;43:9881–91.
- [26] Grohens Y, Hamon L, Reiter G, Soldera A, Holl Y. *Europhysics J E* 2002;8:217–24.
- [27] Etienne S, Becker C, Ruch D, Grignard B, Cartigny C, Detrembleur C, et al. *J Therm Anal Calorim* 2007;87:101–4.
- [28] Chazeau L, Gauthier C, Vigier G, Cavaillé JY. *Handbook of organic-inorganic hybrid materials and nanocomposites*, vol. 2; 2003. 63–111.
- [29] Dalmas F, Cavaillé JY, Gauthier C, Chazeau L, Dendievel R. *Comp Sci Tech* 2007;67:829–39.
- [30] Chabert E, Bornert M, Bourgeat-Lami E, Cavaillé JY, Gauthier C, Dendievel R, et al. *Mater Sci Eng* 2004;381:320–30.
- [31] Chevigny C, Jouault N, Dalmas F, Boué F, Jestin J. *J Poly Sci Part B* 2011;49:781–91.
- [32] Takayanagi M, Vemura S, Minani SJ. *Poly Sci Part C* 1964;5:113.
- [33] Cassagnau P. *Polymer* 2003;44:2455–62.
- [34] Krishnamoorti R, Giannelis EP. *Macromolecules* 1997;30:4097–102.
- [35] Du F, Scogna RC, Zhou W, Brand S, Fischer JE, Winey KI. *Macromolecules* 2004;37:9048–55.
- [36] Pryamitsyn V, Ganesan V. *Macromolecules* 2006;39:844–56.
- [37] Kropka JM, Putz KW, Pryamitsyn V, Ganesan V, Green PF. *Macromolecules* 2007;40:3113–27.
- [38] Sargsyan A, Tonoyan A, Davtyan S, Schick C. *Eur Polym J* 2007;43:3113–27.
- [39] Liu J, Zhang L, Cao D, Wang W. *Phys Chem Chem Phys* 2009;11:11365–84.
- [40] Bogoslovov RB, Roland CM, Ellis AR, Randall AM, Robertson CG. *Macromolecules* 2008;41:1289–96.
- [41] Jouault N, Dalmas F, Said S, Di Cola E, Schweins R, Jestin J, et al. *Phys Rev E* 2010;82:031801.
- [42] Sarvestani AS, Picu CR. *Polymer* 2004;45:7779–90.
- [43] Kropka JM, Sakai VG, Green PF. *Nano Lett* 2008;8:1061–5.
- [44] Leibler L, Rubinstein M, Colby RH. *Macromolecules* 1991;24:4701–7.
- [45] Robertson CG, Rackaitis M. *Macromolecules* 2011;44:1177–81.
- [46] Termonia Y. *Polymer* 2010;51:4448–51.
- [47] Zhang Q, Archer LA. *Langmuir* 2002;18:10435–42.
- [48] Sternstein SS, Zhu AJ. *Macromolecules* 2002;35:7262–73.
- [49] Gonzalez-benito J, Gonzalez-Gaitano G. *Macromolecules* 2008;41:4777–85.